Journal of the Korean Nuclear Society
Volume 36, Number 3, pp.276~284, June, 2004

〈Technical Note〉

Evaluation of the TEXAS-V Fragmentation Models Against Experimental Data

Jin H. Song and Ik K. Park
Korea Atomic Energy Research Institute
150 Deokjin-dong, Yuseong-gu, Daejeon 305-353, Korea

Sunchai Nilsuwankosit
Department of Nuclear Technology, Faculty of Engineering,
Chulalongkorn University,Bangkok, Thailand 10330
dosa@kaeri.re.kr

(Received November 12, 2003)

Abstract

This paper presents the results of the TEXAS-V computer code simulations of FARO L-14, L-28, and L-33. The old break-up model and new break-up model are tested to compare the respective simulations of each. As these experimental data sets cover a wide range of ambient pressures, sub-cooling of the water pool, and the melt jet diameters, the results of the simulations will be beneficial in assessing the TEXAS-V code' s capability to predict the steam explosion phenomena in a prototypical reactor case. The current model was found to have some deficiencies, and the modules for the fragmentation, the equation of state, and the interfacial area for each flow regime in TEXAS-V were improved for the simulation of FARO L28 and FARO L-33.

Key Words : steam explosion, break up, TEXAS-V, FARO, premixing.

1. Introduction

During a severe accident in a nuclear reactor a steam explosion could occur if there is an interaction between the molten core and a coolant. Though many studies have sought to understand the fundamental mechanisms underlying the phenomena and to quantify the risk of steam explosion, by either an analytical approach or an experimental approach, there is no reliable way to predict a steam explosion risk at the reactor scale. The explosivity of the reactor material remains a fundamental issue, and the various approaches at quantifying the steam explosion load have resulted in only high degrees of uncertainty and large deviations. As a result, an international collaboration on Fuel Coolant Interaction (FCI) research, named SERENA [1], was launched to reach concurrence on the understanding of FCI processes and energetics. Accordingly, experimental research on steam explosion, using prototypical material is under way [2, 3].

The present paper discusses the results of the simulations of the FARO experiments by the TEXAS-V computer code [4, 5], as part of the SERENA program. The experiments selected are FARO L-14 [6], L-28 [7], and L-33 [8]. The focus of this paper is on assessing the capability of the fragmentation model of the TEXAS-V in predicting the premixing phase.

As shown in Table 1, these experiments cover a wide range of initial and boundary conditions. These experiments used the TERMOS [8] test section. The melt composition is 20w% UO_2 and 80w% ZrO_2. The L-14 experiment was performed at high pressure, while the L-28 and L-33 experiments were performed at a low pressure. The water pool of L-14 and L-28 was at the saturated condition, while the pool water of FARO L-33 was highly sub-cooled. The melt jet diameter of FARO L-14 is two times larger than that of FARO L-28 and FARO L-33. With these different conditions, the effects of the ambient pressures, the sub-cooling, and the melt jet diameters on the TEXAS-V fragmentation model can be systematically investigated in this paper. The knowledge gained in these efforts will be very beneficial in assessing the TEXAS-V code's capability in predicting the steam explosion phenomena in a prototypical reactor case.

Table 1. Comparison of Major Parameters Between FARO L-14, L-28 and L-33

	L-14	L-28	L-33
Mass (kg)	125	175	92
Release diameter (m)	0.1	0.05	0.05
Pressure (MPa)	5.0	0.51	0.22
Sub-cooling (K)	0	0	104
Water Depth (m)	2.05	1.44	1.45
Gas volume (m3)	1.26	3.528	3.492
Water volume (m3)	0.798	0.564	0.628
Melt delivery (s)	1.0	5.21	1.125

2. TEXAS-V Fragmentation Model

The key constitutive relation in TEXAS-V is the hydrodynamic fuel fragmentation model. The current version [4] has an option for the old break up model by Rayleigh-Taylor instability (RT) alone and for the new break up model, which has three break-up mechanisms.

2.1. Old Break-Up Model

The basic fragmentation mechanism employed is Rayleigh-Taylor instability, developed by Chu and Corradini [9], based on Pilch's original concept [10] of a multi-step fragmentation theory for liquid particles. The model considers the fuel particles to be deformed and dynamically fragmented into a discrete number of particles of smaller sizes. The correlation of this theoretical model reads as:

$$D(T^+)=D(0)\exp(-C_1(T^+)C_2WeC^3) \quad (1)$$

By averaging the fragmentation rate, the above equation can be simplified to a linear, time-independent form, as:

$$D_f^{n+1} = D_f^n (1-C_oT^+We^{0.25}) \quad (2)$$

where the superscripts n, n+1 designate the old and the new time step values; We is the Weber number for the fuel particles; T^+ is a dimensionless time step; and C_o is a constant:

$$We= \rho_c U_{rel}{}^2 D_f^n \quad (3)$$

$$\Delta T^+ = U_{rel} (t^{n+1} - t^n)/ D_f^n (\rho_c/\rho_f)^{1/2} \quad (4)$$

$$C_o= 0.1093 - 0.0785 (\rho_c/\rho_f)^{1/2} \quad (5)$$

where U_{rel} is the relative velocity; D_f is the fuel diameter; and ρ_f and ρ_c are the densities of fuel and coolant respectively. The break up model is

applied to the free particles and the first NBREAK number of injected particles.

2.2. New Break-Up Model

In order to simulate the complete process of the fragmentation of the fuel, during an interaction with the coolant, three mechanisms are proposed [11, 12, 13]. Due to the different characteristic lengths and conditions of each, these mechanisms are assumed to be responsible for the fragmentation in different parts of the fuel jet. The first mechanism is Raleigh-Taylor instability (RT). This mechanism was initially employed in TEXAS and is considered the major factor for the fragmentation, particularly when the fuel jet is fragmented into small particles, which makes RT more effective due to its small characteristic length. For the part of the fuel jet that is still intact, the Kevin-Helmholtz instability (KH), is considered to be the major factor for its fragmentation. The third mechanism, boundary layer (BL) stripping, is considered responsible for the fragmentation of the frontal part of the fuel jet, due to its direct impact with the coolant.

Rayleigh-Taylor instability: Equations (1) to (5) given in the previous section are still applicable. The break up model applies to the first NBREAK number of the injected particles and the free particles generated from the intact jet by the RT, KH, or BL models.

Kelvin-Helmholtz instability: The model proposed by Epstein and Fauske [12] is used. In this model, there are two sets of equations to be applied based on the condition of the coolant surrounding the fuel. If the coolant is mostly liquid (void fraction < 0.2, by default), the condition is considered that of a "thin film": only a very thin vapor film is present over the surface of the fuel. In such a case, the major effect is due to the liquid itself. On the other hand, if the coolant is a mixture of vapor and liquid (void fraction > 0.2) then the "thick film" condition is assumed. In this condition, both the liquid and the vapor can affect the fragmentation. The equations for these two conditions are as following.

Thin Film

$$n_{max}^2=\rho_f\rho_l k_{min}^2(u_l-u_f)^2/(\rho_f-\rho_l)^2-(\sigma_f+\sigma_l)k_{min}^3/(\rho_f+\rho_l) \quad (6)$$

$$k_{min}=2/3\rho_f\rho_l(u_l-u_f)^2/(\sigma_f+\sigma_l)/(\rho_f+\rho_l) \quad (7)$$

Thick Film

$$n_{max}^2=\rho_f\rho_l k_{min}^2(u_l-u_f)^2/(\rho_f-\rho_l)^2-\sigma_f k_{min}^3/(\rho_f+\rho_l) \quad (8)$$

$$k_{min}=2/3\rho_f\rho_l(u_l-u_f)^2/(\rho_f+\rho_l)/\sigma_f \quad (9)$$

with $\lambda_{max}=2\pi/k_{min}$, the fragmentation rate is calculated as

$$dm_{KH}/dt=C_{KHA}\rho_f n_{max}\lambda_{max} \quad (10)$$

where C_o is to be determined by the experiments, and A is the surface area of the jet. For the particles generated from the fragmentation, their sizes are assumed to be that given by the critical Weber number:

$$We_{critical}\sim 10\text{-}12,\ D_{critical}=\sigma_f We_{critical}/(\rho_c u_{rel}^2) \quad (11)$$

Boundary Layer Stripping: This model assumes that the layer of the melt formed at the frontal part of the jet would flow from the frontal part of the jet to the side and would then be stripped away by the surrounding fluid. In this scheme, a boundary layer profile over the melt is assumed. With this assumption, Chu et al. [13] estimated the erosion rate as

$$d(m_{BL})/dt=\rho_f\int 2\pi u r dr \quad (12)$$

$$\delta=(2\pi R\nu_f/u_{rel})^{1/2} \quad (13)$$

$$u = u_{rel}\, e^{(r-R)/\delta} \qquad (14)$$

The size of the particles generated is also assumed to be that generated by equation (11). The integration in equation (6) is from R-δ to R.

General remark: The melt jet injection is simulated by an injection of a group of spherical particles. Each particle is fragmented by various mechanisms. The fragmented particles generally belong to the same group. The broken fuel particles can be divided into two groups, only when the number of particles in the original group exceeds the given number of *maxn*, specified by the user for the efficiency of the numerical algorithm. The new group has the same property as the original, except that the location is on top of the original group. Each group has a number of particles having the same temperature and velocity that are subject to the same fragmentation type.

3. Simulation of FARO L-14

The pressure responses of FARO L-14 using the Raleigh Taylor break up model and the new break up model are compared with the experimental data in Fig. 1. It is shown that the overall response of the TEXAS-V simulation is in good agreement with the experimental data. Though the RT break up model is simple and straightforward, the calculated pressure is quite close to that of the experimental data. The pressure calculated by the new break up model is higher than that of either the L14 test data or the old break up model. The input data used for the new break up model are C_{KH}=0.01, *maxn*=1.e6, NBREAK=5, minimum bubble/ droplet radius R=0.001, which will be discussed in section 5.

There is a slight difference in pressure response, due to the different break up mechanism. The comparison of the particle surface area is shown in Fig. 2.

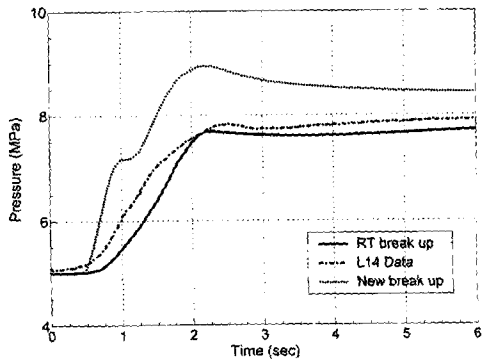

Fig. 1. Comparison of Pressure Response

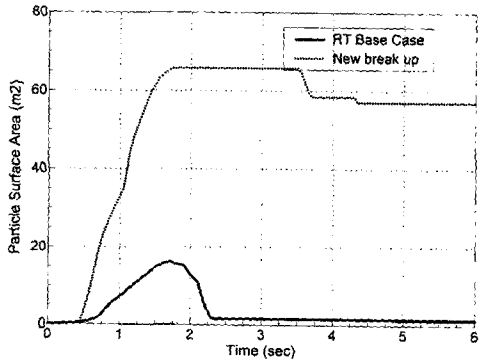

Fig. 2. Comparison of Particle Surface Area

The particle surface area for the RT increases for 1.7 seconds and then decreases as the melt jet injection stops at about 1 second. The combination of particles at the bottom begins when the particles accumulate at the bottom. The total surface area for the new break up model is much bigger than that of RT, because of a large number of small-sized particles generated by the BL and KH mechanisms. The small, broken up particles take longer to reach the bottom, which results in a much longer time for the decrease in the particle area.

The trajectory of the leading edge is shown in Fig. 3. The old break up model resulted in a much longer time to hit the bottom, as the leading

particle became very small due to continuous fragmentation by RT. However, the leading edge in the new break up mechanism, which is prone to BL only, has a larger size. This resulted in a faster time for the leading edge to hit the bottom. The vaporization rate is consistent with the pressurization behavior, as shown in Fig.4.

Figure 5 shows the particle surface area resulting from each break up mechanism in the new break up model. After two seconds, either the particles have cooled below the melting temperature or they have reached the bottom level. Subsequently, the surface area for the heat transfer does not increase.

The surface area marked KH is the surface area of the particles remains as a part of the intact melt jet. It increases during melt delivery until 1 second. After 1 second, it decreases, as the particles hit the bottom of the test section. The front of the jet still experiences the BL stripping, until the final particle injected hits the bottom; however the amount of break up by BL stripping is much less than the others. The particles indicated as RT are generated by the RT, KH, or BL fragmentation mechanisms. The number of free particles is reduced rapidly after melt jet delivery has stopped. At about 1.0 second, there is a short halt in the increase of the particle area. It corresponds to the halt in the increase in pressurization. However, as this phenomenon does not appear in the test data, this may be an artificial effect caused by the new break-up model.

As the melt accumulates at the bottom, the increase in liquid temperature is most abrupt at the lower cell, while the changes in the upper cells are moderate. The void fraction near the middle of the pool ranges from 0.4 to 0.6. The void fraction at lower locations is relatively larger.

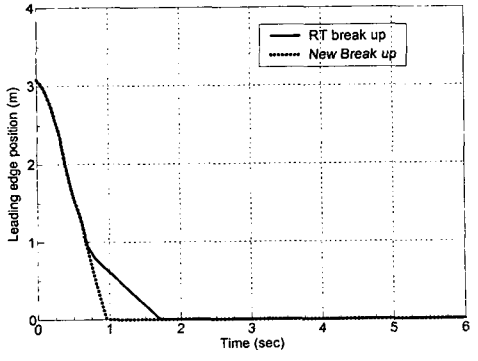

Fig. 3. Trajectory of the Leading Edge for FARO L-14

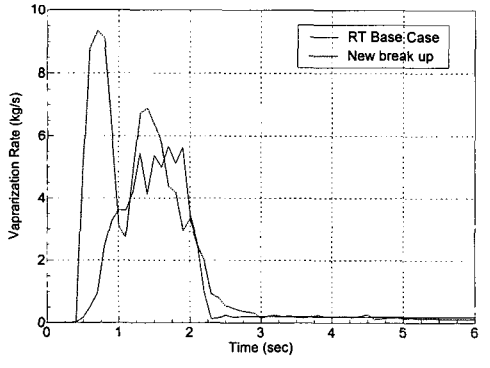

Fig. 4. Vaporization Rate

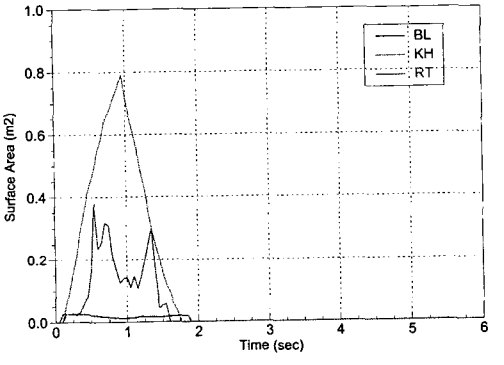

Fig. 5. Surface Area for Each Fragmentation

4. Simulation of FARO L-28

The modules for the fragmentation, the equation of state, and the interfacial area for each flow regime in TEXAS-V are improved for the

simulation of FARO L28 and FARO L-33, as discussed in section 5. The trends of the TEXAS-V simulation for these new tests are quite different from that of the ISP 39 problem of FARO L14, in the sense that the old break-up model and new break-up model provided quite different results. The main differences between FARO L-14 and FARO L28 are the ambient pressures and melt jet diameters.

The base case for the new break up model uses C_{KH}=0.12, NBREAK=5, *maxn*=1.*e*8, minimum bubble/droplet radius R=0.005. Except for the c(141) coefficient, the same input data are used for the case as the old break up model. The pressure responses for the base case with the new break-up model and the old break-up model are shown in Fig. 6. Surprisingly, the trends are very different from those of FARO L-14. The case with the old-break up model does not result in any substantial pressurization. For the new break-up model, we had to increase the proportional constant C_{KH} for the KH break-up mechanism to obtain a reasonable pressurization. It could be due either to a deficiency in the heat transfer model at a low pressure or to the break up mechanism itself. Here, the focus is on the effect of the break up mechanism.

The comparison of particle surface area for both mechanisms is shown in Fig. 7. The trends are

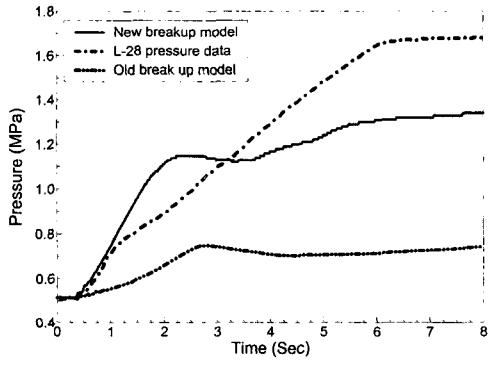

Fig. 6. Pressure Responses for FARO L-28

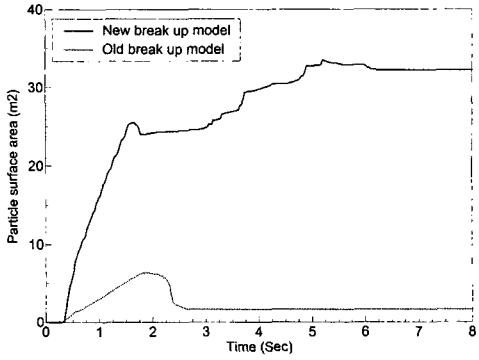

Fig. 7. Comparison of Particle Surface Area

quite similar to those of FARO L-14. The melt jet delivery for FARO L-28 stops at 5.21 seconds. The particle surface area decreases when the last particle hits the bottom in the case of the new break-up model.

For the base case, the vaporization and the condensation rate and particle surface area for each fragmentation mechanism are shown in Fig. 8 and Fig. 9 respectively. The behaviour of the vaporization and the condensation rate are consistent with pressure response. When there is large amount of condensation, the pressurization stops temporarily. This phenomenon seems to be closely related to the fragmentation mechanism.

Figure 9 shows the surface area for each fragmentation. The response of coherent melt jet prone to the KH mechanism is consistent with

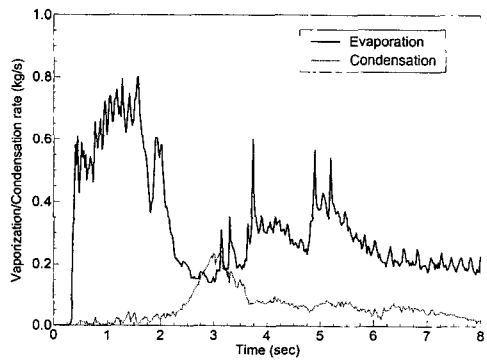

Fig.8. Vaporization and Condensation Rate

melt jet delivery. It becomes zero when the last particle hits the bottom. During the early phase, the coherent melt jet increases as the feeding of particles exceeds the fragmentation by KH. The fragmented particles become free, which results in an increase in the particle area for RT. When the fragmented particles cool down rapidly, the particle area prone to RT decreases.

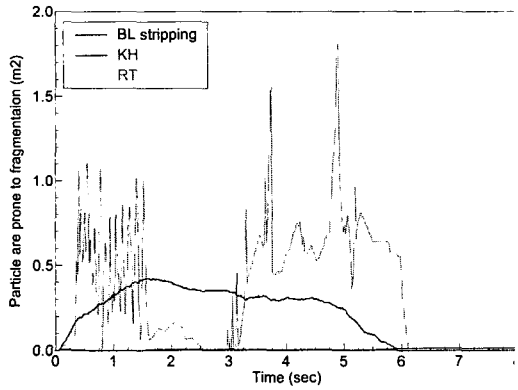

Fig. 9. Surface Area for Each Fragmentation

The number of hot free particles, whose temperatures are above the melting temperature, disappears around 3 second. At this time, the effect of condensation occurring in a cell with a two-phase mixture becomes comparable to that of the vaporization rate. As a result, the pressure does not change. However, this kind of pressure halt does not appear in the experimental data, suggesting that the break-up model needs to be improved. It is shown that BL stripping mechanism is negligible.

5. Simulation of FARO L-33

5.1. Interfacial Area

In TEXAS-V there are three flow regimes of bubbly, intermittent, and mist flow. It is assumed that the dispersed phase consists of bubbles and/or droplets of a uniform size. The interfacial area of the dispersed phase is determined by the void fraction and the droplet/bubble diameter. The radius used in determining the surface area is the minimum radius among the radii determined by the critical Weber number, the radius equivalent to the single bubbles occupying the whole volume, and the size of the cell.

When either the slip velocity between the phases or the fraction of the dispersed phase is small, the appropriate radius should be specifically given. A typical number of R=0.001 is used for the simulation of FARO L-14. However, when this number was used for the FARO L-28 and L-33 simulations, unrealistic depressurization occurred during melt jet delivery. It turned out that this depressurization was due to excessive condensation. When the system pressure is low, the bubble size of the bubbly flow increases. As a result, larger bubble sizes should be used for low-pressure tests of FARO L-28 and L-33. This effect is due the combined effects of fine particles and increased condensation potential. The TEXAS-V logic for the fragmentation model and for determining the interfacial area are modified to handle this situation.

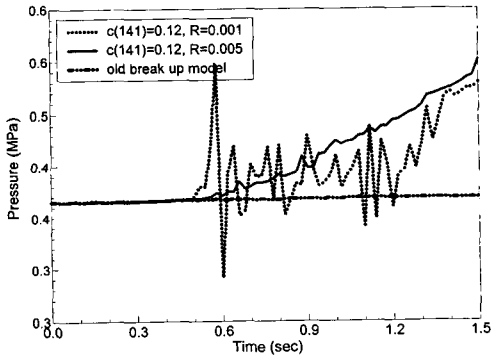

Fig. 10. Pressure Response for FARO L-33

The input data selected for the base case for FARO L-33 simulation are CKH=0.12, NBREAK=5, maxn=1.e6. Atmospheric pressure

is taken as the reference pressure. The most important parameters are the minimum radius for the bubbly flow and droplet flow, selected as 0.005 instead of 0.001.

The pressure response, evaporation, and condensation rate for those cases are shown below. The measured pressure for FARO L-33 increased from 4.1 bar to 4.4 bar until 1.125 seconds, when a steam explosion was set off with an external trigger. The simulations are performed until 1.5 seconds, for convenience, as the behavior due to the explosion is not handled in this paper.

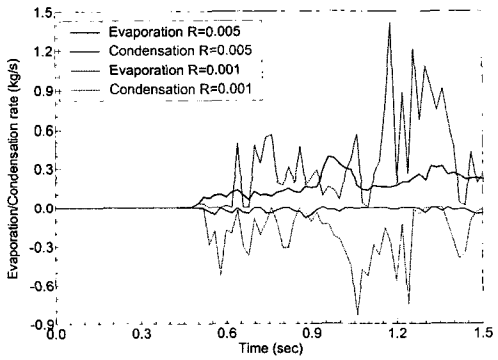

Fig. 11. Vaporization and Condensation Rate

The case of using a small radius results in unrealistic oscillations in pressure, though the average pressure behavior is the same as R=0.005, which is the minimum bubble and/or droplet radius. The case with a small bubble/droplet radius results in a higher condensation rate, which in turn highly increases the evaporation rate to offset the condensation. The exaggerated oscillations in the evaporation and condensation rates result in a failure of numerical convergence.

5.2. Effect of Fine Particles

When the new break-up model is employed,

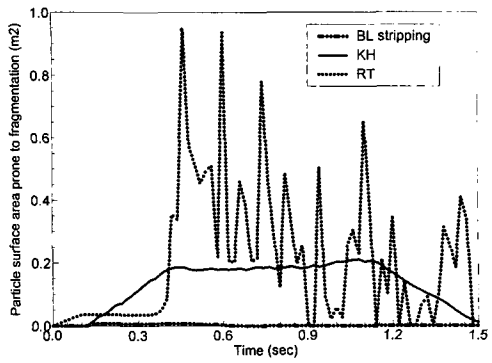

Fig. 12. Surface Area for Each Fragmentation

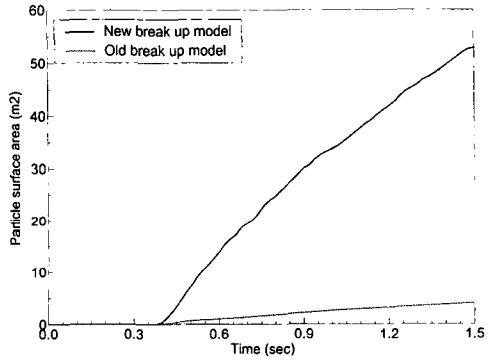

Fig. 13. Comparison of Particle Surface Area

small particles are generated. They lose heat rapidly and the temperature falls to that of the surrounding fluid. If the pool water is highly sub-cooled, there is a chance that the particle temperature will fall below the saturation temperature.

The original TEXAS-V logic has a deficiency in handling this situation. The code failed during the simulation of FARO L-33. This failure does not happen during the simulations of FARO L-28 and FARO L-14.

Therefore, the TEXAS-V logic has been improved to handle this situation.

The behavior of the break-up mechanism can be estimated by plotting the particle surface area for each break up mechanism for the base case, as in Fig. 12. A comparison of the particle areas between the old break up model and new break up

model is shown in Fig. 13. The trends are very similar to that of FARO L-28. The melt jet injection is terminated at 1.125 second.

6. Conclusions

By performing simulations for FARO L-14, L-28, and L-33 experiments, the capability and the limitations of the TEXAS-V fragmentation models for the premixing phase were investigated. By improving the deficiencies in the modules for the fragmentation, the equation of state, and the interfacial area for each flow regime, successful simulations of FARO L-14, L-28, and L-33 were made possible. As those experimental sets cover a wide range of initial and boundary conditions, the results of the simulations will be very useful for further application of the TEXAS-V at the reactor scale.

Acknowledgments

The authors would like to thank the Ministry of Science and Technology, Republic of Korea, for its support of this study.

References

1. Magallon et. al, 2001, Proposal for a OECD research programme on fuel-coolant interaction-Steam Explosion Resolution for Nuclear Applications (SERENA).
2. J. H. Song et. al., Spontaneous steam explosions observed in the fuel coolant interaction experiments using reactor materials, Journal of Korean Nuclear Society, Vol. 33(4), 344-357, 2002.
3. J. H. Song et. al., Fuel coolant interaction experiments in TROI using a UO2/ZrO2 mixture, Nuclear Engineering and Design, 222, pp.1-15, 2003.
4. Chu, C. C., 1986, One-Dimensional Transient Fluid Model for Fuel-Coolant Interaction Analysis, PhD Thesis, University of Wisconsin.
5. Corradini, M. L., El-Beshbeeshy, Nilsuwankosit, S., Tang, J., Fuel Fragmentation model advances using TEXAS-V, 1997, Proceedings of the OECD/CSNI specialists meeting on fuel-coolant interactions, pp.733-738, Tokai Mura, Japan.
6. Annunziato, A., Addabbo, A., Leva, G., 1996, OECD/CSNI international standard problem No. 39 on FARO test L-14, Technical Note No. I.96.64, Joint Research Center.
7. Annunziato, A., Addabbo, A., Magallon, D., 1999, FARO test L-28 quick look report, Tchnical Note I.99.74, Joint Research Center.
8. Annunziato, A., Addabbo, A., Magallon, D., 2000, FARO test L-33 quick look report, Tchnical Note I.00.111, Joint Research Center.
9. Chu, C., C. et al, 1984, A Dynamic Model for Droplet Fragmentation, Trans. of Amer. Nuclear Society, V47, Washington, DC. .
10. Young, M. F., 1982, The TEXAS Code for Fuel-Coolant Interaction Analysis, Proc. ANS/ENS LMFBR Safety Topical Mtg., Lyon-Ecully, France.
11. Tang, J., Corradini, M., L., 1996, Final Technical Report for Fuel-Coolant Interaction Analysis for FARO-LWR Test Interpretation, Nuclear Engineering and Engineering Physics, University of Wisconsin.
12. Epstein, M., Fauske , H., K., 1985, Steam Film Instability and the Mixing of Core Melt Jets and Water, Proceedings of National Heat Transfer Conference, Denver, Colorado, USA.
13. Chu, C., C. et. al., 1995, Ex-Vessel Melt-Coolant Interactions in Deep Water Pool: Studies and Accident Management for Swedish BWRs, Nuclear Engineering Design, vol. 155, p 159-213.